JACS
JOURNAL OF THE AMERICAN CHEMICAL SOCIETY

Article

pubs.acs.org/JACS

Helical Gold Nanorods as Chiral Recognition Nanostructures: A Relativistic Density Functional Theory Study

Xiaojing Liu and Ian P. Hamilton*

Department of Chemistry, Wilfrid Laurier University, Waterloo, N2L 3C5 Ontario, Canada

Supporting Information

ABSTRACT: We establish helical gold nanorods as the first examples of chiral recognition nanostructures by examining the simple chiral molecule CClHDT adsorbed on the helical Au_{40} nanorod. We calculate the vibrational circular dichroism (VCD) spectra of the R and S enantiomers of CClHDT adsorbed on the R (or S) enantiomer of Au_{40} using relativistic density functional theory. The highest adsorption energy is found when the Cl atom of CClHDT binds to a low-coordinated Au atom at the edge of Au_{40}. There are three adsorption modes (essentially identical in energy) corresponding to three orientations of the HDT moiety. We show that, for each adsorption mode, the VCD spectra are distinctly different for the Au_{40}(R)-ClHDT(R) and Au_{40}(R)-CClHDT(S) complexes, and we give a qualitative explanation for this based on the principle of chirality transfer. For comparison with the results for Au_{40}, we calculate the VCD spectra of the R and S enantiomers of CClHDT adsorbed on the achiral Au_{20} tetrahedral cluster. Again, there are three adsorption modes (essentially identical in energy) corresponding to three orientations of the HDT moiety. However, we show that, for each adsorption mode, the VCD spectra are mirror symmetric but otherwise essentially identical for the Au_{20}-CClHDT(R) and Au_{20}-CClHDT(S) complexes. Thus, the inherent chirality of the helical Au_{40} nanorod is essential for its chiral recognition functionality.

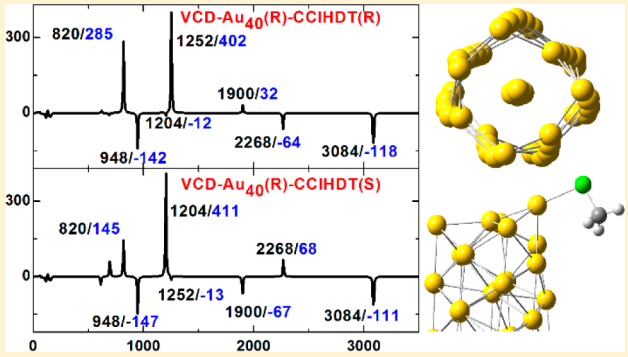

1. INTRODUCTION

Metal clusters have received a great deal of attention due to their electronic and magnetic properties, aromaticity, and catalytic activity, all of which can differ significantly from those of the bulk metal.[1−3] For example, our previous studies have shown that various small metal clusters can activate the inert C−H bond.[4] Also, metal clusters protected by chiral ligands have been used for the synthesis of particular enantiomers.[5−7] Metal colloids, in combination with a chiral modifier, have been used for the asymmetric hydrogenation of ketones.[8,9] Metal clusters which are chiral have unique electronic and magnetic properties that may lead to novel functionality in nanostructured devices.[10]

Vibrational circular dichroism (VCD) is the differential absorbance of left and right circularly polarized light of vibrational transitions in the infrared (IR) region.[11,12] It is a very successful spectroscopic technique for determining the absolute configuration (AC) of chiral molecules. Compared to other more conventional AC determination tools, such as X-ray crystallography, VCD has the advantage of not requiring a single crystal. Another advantage of VCD as an optical spectroscopic method is its ability to register signals from an individual conformer.[12] The reliability of AC determinations using VCD spectroscopy combined with density functional theory (DFT) studies has been solidly established.[13−17]

There are a number of studies in which a ligand-protected gold nanocluster has chirality induced by chiral ligands.[18−22] However, there are only a few studies in which the gold nanocluster is intrinsically chiral. A recent study showed that the Au_{34} anion is potentially chiral.[23] Also, two low-symmetry "disordered" gold structures, Au_{28} and Au_{55}, have been reported to be chiral[24] and the adsorption of chiral molecules on these structures was examined.[25] The helical Au_{40} nanorod, which is inherently chiral, was the focus of our previous study, which established its stability.[26] As discussed in that study, other isomers of Au_{40} are also stable but, in this paper, we exclusively consider the helical Au_{40} nanorod. We recently examined the adsorption of a variety of small molecules on the helical Au_{40} nanorod.[27] Although the Au−S and Au−O bonds are generally weaker than the Au−C and Au−N bonds, we found that adsorption of H_2S or H_2O caused greater distortion of Au_{40} in the binding region than adsorption of CO or NH_3. However, the degree of distortion was always small, and the helical geometry was always retained, demonstrating the stability of the helical Au_{40} nanorod upon complex formation.

Received: August 17, 2014
Published: December 2, 2014

   dx.doi.org/10.1021/ja5084267 | J. Am. Chem. Soc. 2014, 136, 17757−17761

2. COMPUTATIONAL METHODS

We used scalar relativistic DFT as implemented in the Gaussian software package[28] and performed full geometry optimizations for all structures. The optimized geometries are all (local) minima, as confirmed by vibrational frequency analysis. In our DFT calculations, the exchange-correlation functional within the generalized gradient approximation (GGA) was employed. Specifically, we use the Becke exchange functional with the Perdew correlation functional (BP86) that was used in our previous studies.[26,27] We note that some GGA exchange-correlation functionals, and B3LYP in particular, can be problematic for gold clusters because they tend to favor planar geometries[29] and electron affinities are not well reproduced.[30] However, recent results for neutral gold clusters have shown that the BP86 functional gives excellent results for geometries and adsorption energies, and is sufficiently accurate for the neutral gold clusters we consider in this study.[31] As in our previous studies,[26,27] we use the Los Alamos small-core pseudopotential of Hay and Wadt[32] together with the corresponding double-ζ basis set. It is well established that small-core pseudopotentials of this sort can accurately describe relativistic and electron correlation effects in atoms and molecules.[31,33] In addition, vibrational frequencies, infrared spectra, and VCD spectra for the optimized structures are calculated. Our adsorption energies include the dispersion energy, which is evaluated using the D3 method of Grimme et al.,[34] and the basis-set superposition error, which is evaluated using the counterpoise method.[35]

3. RESULTS AND DISCUSSION

The Au_{40} structure has a central strand of five gold atoms along an axis and seven strands of five gold atoms on a coaxial tube as shown in the left panel of Figure 1. The highest adsorption energy is found when the Cl atom of CClHDT binds to a low-coordinated Au atom at the edge of Au_{40} as shown in the right panel of Figure 1.

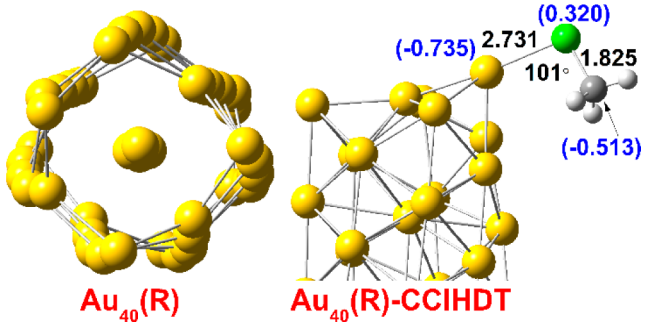

Figure 1. End view of Au_{40}(R) (left panel) and side view of the Au_{40}(R)-CClHDT complex (right panel).

The adsorption energy is calculated to be 13.24 kcal/mol, the Au−Cl bond length is 2.732 Å, the Au−Cl vibrational frequency is 159.05 cm^{-1}, and the Au−Cl−C angle is 101°. Upon adsorption, the C−Cl bond length increases from 1.808 to 1.825 Å and the charge located in the C−Cl bond increases from −0.584 to −0.194.

There are three adsorption modes (I, II, and III), essentially identical in energy, for which the H, D, or T atom, respectively, is oriented away from Au_{40}. Upon adsorption, there is charge transfer from CClHDT to Au_{40} and CClHDT has a positive charge of 0.328. The charge of the C atom increases from −0.653 to −0.513 while that of the Cl atom increases from 0.069 to 0.319 and that of the Au atom at the adsorption site decreases from −0.726 to −0.735. Clearly, polar effects play an important role, weakening the C−Cl bond and strengthening the Cl−Au interaction.

The IR and VCD spectra of Au_{40} are shown in Figure 2. It may be seen that (as expected) the IR spectra of Au_{40}(R) and

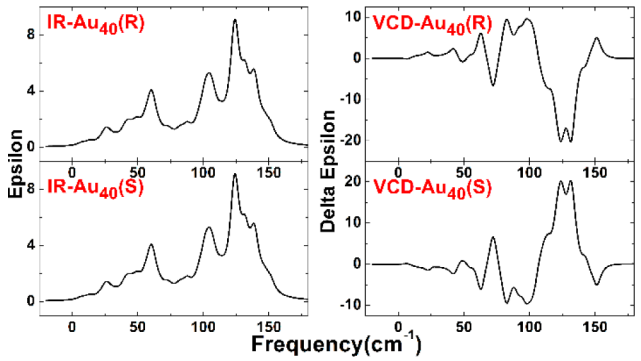

Figure 2. IR spectra (left panels) and VCD spectra (right panels) of Au_{40}(R) and Au_{40}(S).

Au_{40}(S) are essentially identical and the VCD spectra of Au_{40}(R) and Au_{40}(S) (which display both positive and negative Cotton effects) are mirror symmetric but otherwise essentially identical.

The IR spectra of CClHDT and the Au_{40}-CClHDT complexes are shown in Figure 3. We first consider the IR

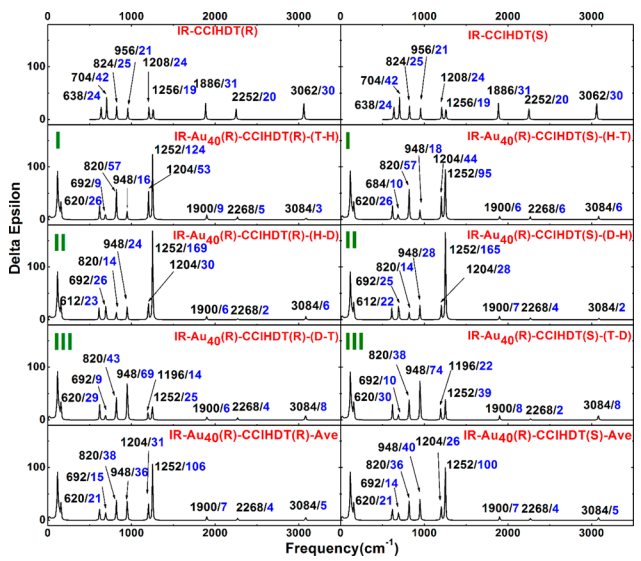

Figure 3. IR spectra of CClHDT(R) and Au_{40}(R)-CClHDT(R) (left panels) and CClHDT(S) and Au_{40}(R)-CClHDT(S) (right panels).

spectra of CClHDT(R) and CClHDT(S) which are shown in the top panels of Figure 3. It may be seen that (as expected) the IR spectra of these two enantiomers are essentially identical. In order of increasing frequency, the first three peaks correspond to the up-and-down vibrations of H/D/T atoms (group 1), the second three peaks correspond to shear vibrations between pairs of these atoms (group 2), and the last three peaks correspond to C−H/D/T stretching vibrations (group 3). Peaks for all three groups have significant intensity.

dx.doi.org/10.1021/ja5084267 | J. Am. Chem. Soc. 2014, 136, 17757−17761

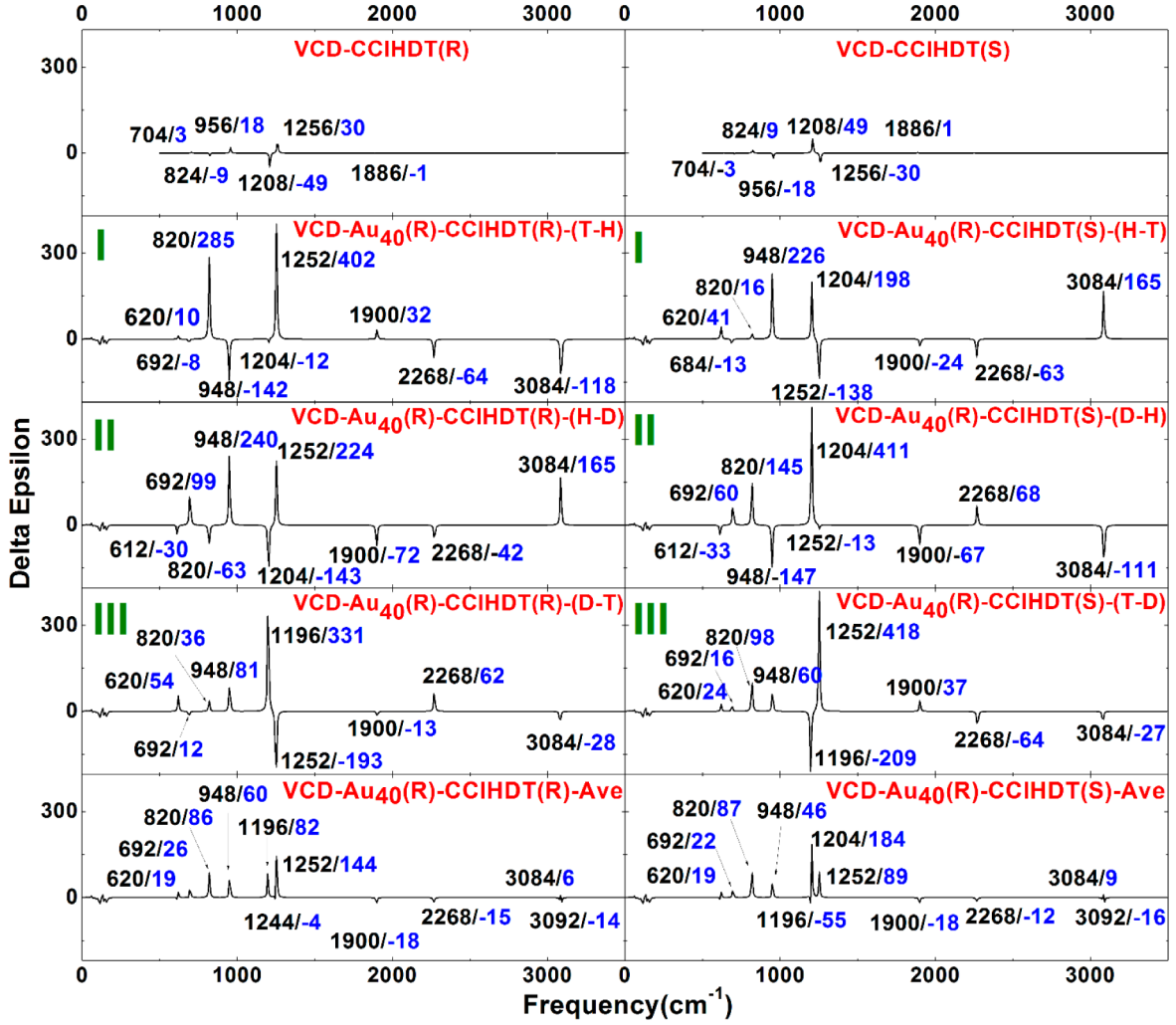

Figure 4. VCD spectra of CClHDT(R) and Au_{40}(R)-CClHDT(R) (left panels), and CClHDT(S) and Au_{40}(R)-CClHDT(S) (right panels).

We now consider the IR spectra of the Au_{40}(R)-CClHDT-(R) and Au_{40}(R)-CClHDT(S) complexes which are shown in the bottom four panels of Figure 3 for adsorption modes I, II, III, and the average of all three. There are large changes in the IR peaks of the Au_{40} moiety and large increases in their intensities (see Figure S2 of the Supporting Information), but we focus on the large changes in the IR spectrum of the CClHDT moiety. Upon adsorption, the group 1 and 2 peaks are red-shifted while the group 3 peaks are blue-shifted. The intensities of the group 2 peaks generally increase while the intensities of the group 3 peaks decrease. It is clear from Figure 3 that the IR spectra of Au_{40}(R)-CClHDT(R) and Au_{40}(R)-CClHDT(S) are significantly different for adsorption modes I, II, and III. However, for a given adsorption mode, the IR spectra of these two enantiomers are essentially identical. This is not surprising because the electric dipole moments of Au_{40}(R)-CClHDT(R) and Au_{40}(R)-CClHDT(S) are the same for a given adsorption mode, but it means that the IR spectra cannot discriminate between adsorption of CClHDT(R) and CClHDT(S).

The VCD spectra of CClHDT and the Au_{40}(R)-CClHDT complexes are shown in Figure 4. We first consider the VCD spectra of CClHDT(R) and CClHDT(S) which are shown in the top panels of Figure 4. It may be seen that (as expected) the VCD spectra of CClHDT(R) and CClHDT(S) are mirror symmetric but otherwise essentially identical. Peaks for group 2 have the greatest intensity, and peaks for group 3 have essentially disappeared.

We now consider the VCD spectra of the Au_{40}(R)-CClHDT(R) and Au_{40}(R)-CClHDT(S) complexes which are shown in the bottom four panels of Figure 4 for adsorption modes I, II, III, and the average of all three. There are large changes in the VCD peaks of the Au_{40} moiety, although no significant changes in their intensities (see Figure S5 of the Supporting Information), but we focus on the large changes in the VCD spectra of the CClHDT moiety. It may be seen that, upon adsorption, the VCD spectra of CClHDT(R) and CClHDT(S) are no longer mirror symmetric. Also, upon adsorption, the VCD intensities generally increase significantly for all three groups.

It is clear from Figure 4 that the VCD spectra for Au_{40}(R)-CClHDT(R) and Au_{40}(R)-CClHDT(S) are significantly different for adsorption modes I, II, and III. Furthermore, for a given adsorption mode, the VCD spectra for Au_{40}(R)-CClHDT(R) and Au_{40}(R)-CClHDT(S) are distinctly different. To demonstrate this, we focus on the group 2 shear vibrations that involve D−T, H−T, and H−D motions. For free CClHDT, these are at 956, 1208, and 1256 cm^{-1}, respectively, and for Au_{40}(R)-CClHDT they are red-shifted to 948, 1204, and 1252 cm^{-1}, respectively. We consider adsorption mode I. For Au_{40}(R)-

dx.doi.org/10.1021/ja5084267 | J. Am. Chem. Soc. 2014, 136, 17757−17761

CClHDT(R), the peak at 1252 cm^{-1} is markedly enhanced, the peak at 948 cm^{-1} is moderately enhanced and the peak at 1204 cm^{-1} has almost disappeared. In contrast, for Au_{40}(R)-CClHDT(S), the peak at 948 cm^{-1} is markedly enhanced and the peaks at 1204 and 1252 cm^{-1} are both moderately enhanced. Distinct differences are also seen for adsorption modes II and III and for the average of all three.

If all three adsorption modes can be observed in the VCD spectra, we propose a semiquantitative procedure for determining the enantiomer of CClHDT which is based on the amplitudes of the group 2 shear vibrations. The largest-amplitude peaks in the VCD spectra are all at the same geometric position in Au_{40}(R)-CClHDT (shown in blue in Figure 5). We suggest that this is because, for this position,

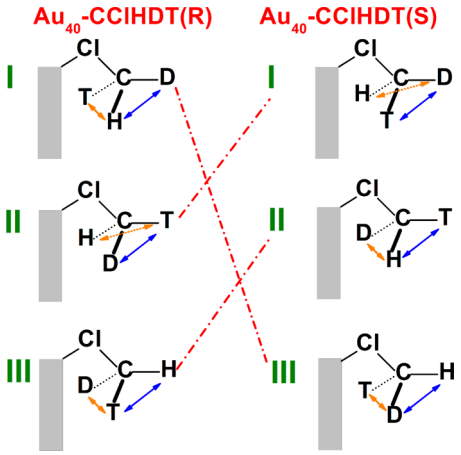

Figure 5. Schematic diagram of positions for largest-amplitude (blue) and smallest-amplitude (orange) peaks of bending vibrations in the VCD spectra.

these atoms of CClHDT are aligned with the helically structured gold atoms of Au_{40}. The smallest-amplitude peaks are at the geometric positions shown in orange in Figure 5. Thus, if the largest-amplitude peak in the experimental VCD spectrum is at 1252 cm^{-1}, then the adsorption mode is either I(R) or III(S) (connected by a dashed red line in Figure 5). Then, if the smallest-amplitude peak is at 1204 cm^{-1}, it is the R enantiomer of CClHDT, and if the smallest-amplitude peak is at 948 cm^{-1} it is the S enantiomer of CClHDT. Corresponding conclusions can be drawn if the largest-amplitude peak in the experimental VCD spectrum is at 1204 or 948 cm^{-1} and, in each case, the enantiomer of CClHDT can be definitively determined.

Thus, for the helical Au_{40} nanorod, the VCD spectra can discriminate between adsorption of CClHDT(R) versus adsorption of CClHDT(S). To our knowledge, this is the first instance in which this capability has been established for a nanostructure.

For comparison with the results for Au_{40}, we consider results for R and S enantiomers of CClHDT adsorbed on the achiral Au_{20} tetrahedral cluster. The Cl atom of CClHDT preferentially binds to a Au atom at the apex of the Au_{20} structure (see Figure S8 of the Supporting Information). There are three adsorption modes (I, II, and III), essentially identical in energy, for which the H, D, or T atom, respectively, is oriented away from Au_{20}. The VCD spectra for Au_{20}-CClHDT(R) and Au_{20}-CClHDT(S) are significantly different for adsorption modes I, II, and III (see Figure S10 of the Supporting Information). However, for a given adsorption mode, the VCD spectra for Au_{20}-CClHDT(R) and Au_{20}-CClHDT(S) are mirror symmetric but otherwise essentially identical. Thus, for the achiral Au_{20} tetrahedral cluster, the VCD spectra cannot discriminate between adsorption of CClHDT(R) and CClHDT(S) and the inherent chirality of the helical Au_{40} nanorod is essential for its chiral recognition functionality.

We now consider the rationale for the differences between the VCD spectra of the Au_{40}(R)-CClHDT(R) and Au_{40}(R)-CClHDT(S) complexes. A quantitative explanation based on the scalar (or dot) product of the electric dipole moment vector and the imaginary part of the magnetic dipole moment vector could be given,[36] but we believe that it is more insightful to give a qualitative explanation based on the principle of chirality transfer (or induced chirality).[37] For the complex of a chiral molecule and an achiral molecule, the vibrations of the achiral molecule are observed in the VCD spectrum. For example, for the Au_{40}(R)-NH_3 complex, the bend and stretching vibrations of NH_3 are observed in the VCD spectrum because there is chirality transfer from Au_{40}(R) to NH_3. For the Au_{40}(R)-CClHDT(R) and Au_{40}(R)-CClHDT(S) complexes, there is a conflict between the chiralities of Au_{40} and CClHDT. There is a qualitative difference between chirality transfer from Au_{40}(R) to the R enantiomer versus the S enantiomer of CClHDT. In principle, there could be chirality transfer from CClHDT to Au_{40} but this is not the case. As shown in Figure S5 of the Supporting Information, the VCD spectra of the Au_{40} moiety are essentially identical for Au_{40}(R)-CClHDT(R) and Au_{40}(R)-CClHDT(S) complexes for all three adsorption modes. It is the ability to perturb the chirality of a species without being perturbed by the chirality of that species that enables Au_{40} to be a quantitative probe of chirality.

The helical gold nanorods are segments of the helical gold nanowires that were studied experimentally by Kondo and Takayanagi.[38] If the helical gold nanowire was to be fragmented and the sections were to be trapped in a cold rare-gas matrix, then the helical gold nanorod-CClHDT complexes could be studied experimentally using the high-resolution technique of matrix isolation VCD spectroscopy, as in a recent experimental study of the lactic acid-NH_3 complex.[39]

In conclusion, we have examined the VCD spectra of the chiral molecule CClHDT adsorbed on the helical Au_{40} nanorod using relativistic density functional theory. We have shown that, for each of the three adsorption modes (and for the average of all three), the VCD spectra are distinctly different for the R and S enantiomers of CClHDT, thereby establishing helical gold nanorods as the first examples of chiral recognition nanostructures.

■ ASSOCIATED CONTENT

Supporting Information

End view of Au_{40}(S) and side view of the Au_{40}(S)-CClHDT(S) complex; enlarged IR spectra of Au_{40}(R) moiety in Au_{40}(R)-CClHDT(R)(S); enlarged IR spectra of Au_{40}(S) moiety in Au_{40}(S)-CClHDT(R)(S); IR spectra of Au_{40}(S)-CClHDT(R)-(S); enlarged VCD spectra of Au_{40}(R) moiety in Au_{40}(R)-CClHDT(R)(S); enlarged VCD spectra of Au_{40}(S) moiety in Au_{40}(S)-CClHDT(R)(S); IR spectra of Au_{40}(S)-CClHDT(R)-(S); VCD spectra of Au_{40}(S)-CClHDT(R)(S); Side view of Au_{20}-CClHDT complex; IR spectra of Au_{20}-CClHDT(R)(S); VCD spectra Au_{20}-CClHDT(R). This material is available free of charge via the Internet at http://pubs.acs.org.

dx.doi.org/10.1021/ja5084267 | J. Am. Chem. Soc. 2014, 136, 17757−17761

AUTHOR INFORMATION

Corresponding Author

ihamilton@wlu.ca

Notes

The authors declare no competing financial interest.

ACKNOWLEDGMENTS

I.P.H. acknowledges support from NSERC, Compute Canada, Sharcnet and Wilfrid Laurier University.

REFERENCES

(1) Daniel, M. C.; Astruc, D. *Chem. Rev.* **2004**, *104*, 293.
(2) Boldyrev, A. I.; Wang, L. S. *Chem. Rev.* **2005**, *105*, 3716.
(3) Kulkarni, A.; Lobo-Lapidus, R. J.; Gates, B. C. *Chem. Commun.* **2010**, *46*, 5997.
(4) Liu, X. J.; Zhang, X.; Han, K. L.; Xing, X. P.; Sun, S. T.; Tang, Z. C. *J. Phys. Chem. A* **2007**, *111*, 3248. Liu, X. J.; Yang, C. L.; Zhang, X.; Han, K. L.; Tang, Z. C. *J. Comput. Chem.* **2008**, *29*, 1667. Liu, X. J.; Han, K. L.; Sun, S. T.; Tang, Z. C.; Qin, Z. B.; Cui, Z. F. *J. Phys. Chem. A* **2008**, *112*, 6850. Liu, X. J.; Li, B.; Han, K. L.; Sun, S. T.; Xing, X. P.; Tang, Z. C. *Phys. Chem. Chem. Phys.* **2009**, *11*, 1043. Liu, X. J.; Hamilton, I. P.; Han, K. L.; Tang, Z. C. *Phys. Chem. Chem. Phys.* **2010**, *12*, 10602.
(5) Dolamic, I.; Knoppe, S.; Dass, A.; Bürgi, T. *Nat. Commun.* **2012**, *3*, 798.
(6) Davis, A. V.; Fiedler, D.; Ziegler, M.; Terpin, A.; Raymond, K. N. *J. Am. Chem. Soc.* **2007**, *129*, 15354.
(7) Gautier, C.; Bürgi, T. *J. Am. Chem. Soc.* **2008**, *130*, 7077.
(8) Fraile, J. M.; García, J. I.; Mayoral, J. A. *Chem. Rev.* **2009**, *109*, 360.
(9) Pârvulescu, V. I.; Hardacre, C. *Chem. Rev.* **2007**, *107*, 2615.
(10) Naaman, R., Beratan, D. N., Waldeck, D. H., Eds. *Electronic and Magnetic Properties of Chiral Molecules and Supramolecular Architectures*; Springer-Verlag: Berlin, 2011.
(11) Yang, G. C.; Xu, Y. J. *Top. Curr. Chem.* **2011**, *298*, 189.
(12) Stephens, P. J.; Devlin, F. J.; Pan, J. J. *Chirality* **2008**, *20*, 643.
(13) Merten, C.; Hyun, M. H.; Xu, Y. J. *Chirality* **2013**, *25*, 294.
(14) Merten, C.; Amkreutz, M.; Hartwig, A. *Phys. Chem. Chem. Phys.* **2010**, *12*, 11635.
(15) Stephens, P. J.; Devlin, F. J. *Chirality* **2000**, *12*, 172.
(16) Kwit, M.; Rozwadowska, M. D.; Gawronski, J.; Grajewska, A. *J. Org. Chem.* **2009**, *74*, 8051.
(17) Batista, J. M., Jr.; Batista, A. N. L.; Rinaldo, D.; Vilegas, W.; Cass, Q. B.; Bolzani, V. S.; Kato, M. J.; López, S. N.; Furlan, M.; Nafie, L. A. *Tetrahedron: Asymmetry* **2010**, *21*, 2402.
(18) Schaaff, T. G.; Whetten, R. L. *J. Phys. Chem. B* **2000**, *104*, 2630.
(19) Yao, H.; Miki, K.; Nishida, N.; Sasaki, A.; Kimura, K. *J. Am. Chem. Soc.* **2005**, *127*, 15536.
(20) Gautier, C.; Bürgi, T. *J. Am. Chem. Soc.* **2006**, *128*, 11079. Dolamic, I.; Knoppe, S.; Knoppe, S.; Dolamic, I.; Dass, A.; Bürgi, T. *Angew. Chem., Int. Ed.* **2012**, *51*, 7589.
(21) Sánchez-Castillo, A.; Noguez, C.; Garzón, I. L. *J. Am. Chem. Soc.* **2010**, *132*, 1504.
(22) Lopez-Acevedo, O.; Tsunoyama, H.; Tsukuda, T.; Häkkinen, H.; Aikens, C. M. *J. Am. Chem. Soc.* **2010**, *132*, 8210.
(23) Lechtken, A.; Schooss, D.; Stairs, J. R.; Blom, M. N.; Furche, F.; Morgner, N.; Kostko, O.; Von Issendorff, B.; Kappes, M. M. *Angew. Chem., Int. Ed.* **2007**, *46*, 2944.
(24) Garzón, I. L.; Reyes-Nava, J. A.; Rodríguez-Hernández, J. I.; Sigal, I.; Beltrán, M. R.; Michaelian, K. *Phys. Rev. B* **2002**, *66*, 073403. Garzón, I. L.; Beltrán, M. R.; González, G.; Gutíerrez-González, I.; Michaelian, K.; Reyes-Nava, J. A.; Rodríguez-Hernández, J. I. *Eur. Phys. J. D* **2003**, *24*, 105.
(25) López-Lozano, X.; Pérez, L. A.; Garzón, I. L. *Phys. Rev. Lett.* **2006**, *97*, 233401.
(26) Liu, X. J.; Hamilton, I. P.; Krawczyk, R. P.; Schwerdtfeger, P. *J. Comput. Chem.* **2012**, *33*, 311.
(27) Liu, X. J.; Hamilton, I. P. *J. Comput. Chem.* **2014**, *53*, 1967.
(28) Frisch, M. J.; Trucks, G. W.; Schlegel, H. B.; Scuseria, G. E.; Robb, M. A.; Cheeseman, J. R.; Scalmani, G.; Barone, V.; Mennucci, B.; Petersson, G. A.; Nakatsuji, H.; Caricato, M.; Li, X.; Hratchian, H. P.; Izmaylov, A. F.; Bloino, J.; Zheng, G.; Sonnenberg, J. L.; Hada, M.; Ehara, M.; Toyota, K.; Fukuda, R.; Hasegawa, J.; Ishida, M.; Nakajima, T.; Honda, Y.; Kitao, O.; Nakai, H.; Vreven, T.; Montgomery, J. A., Jr.; Peralta, J. E.; Ogliaro, F.; Bearpark, M.; Heyd, J. J.; Brothers, E.; Kudin, K. N.; Staroverov, V. N.; Kobayashi, R.; Normand, J.; Raghavachari, K.; Rendell, A.; Burant, J. C.; Iyengar, S. S.; Tomasi, J.; Cossi, M.; Rega, N.; Millam, J. M.; Klene, M.; Knox, J. E.; Cross, J. B.; Bakken, V.; Adamo, C.; Jaramillo, J.; Gomperts, R.; Stratmann, R. E.; Yazyev, O.; Austin, A. J.; Cammi, R.; Pomelli, C.; Ochterski, J. W.; Martin, R. L.; Morokuma, K.; Zakrzewski, V. G.; Voth, G. A.; Salvador, P. J.; Dannenberg, J.; Dapprich, S.; Daniels, A. D.; Farkas, Ö.; Foresman, J. B.; Ortiz, J. V.; Cioslowski, J.; Fox, D. J. *Gaussian 09*, revision A.1; Gaussian, Inc.: Wallingford CT, 2009.
(29) Johansson, M. P.; Lechtken, A.; Schooss, D.; Kappes, M. M.; Furche, F. *Phys. Rev. A* **2008**, *77*, 053202. Ferrighi, L.; Hammer, B.; Madsen, G. K. H. *J. Am. Chem. Soc.* **2009**, *131*, 10605.
(30) Lee, D.; Furche, F.; Burke, K. *J. Phys. Chem. Lett.* **2010**, *1*, 2124.
(31) Assadollahzadeh, B.; Schwerdtfeger, P. *J. Chem. Phys.* **2009**, *131*, 064306.
(32) Hay, P. J.; Wadt, W. R. *J. Chem. Phys.* **1985**, *82*, 299.
(33) Schwerdtfeger, P. *Phys. Scr.* **1987**, *36*, 453. Schwerdtfeger, P.; Fischer, T.; Dolg, M.; Igel-Mann, G.; Nicklass, A.; Stoll, H.; Haaland, A. *J. Chem. Phys.* **1995**, *102*, 2050. Leininger, T.; Nicklass, A.; Stoll, H.; Dolg, M.; Schwerdtfeger, P. *J. Chem. Phys.* **1996**, *105*, 1052. Schwerdtfeger, P.; Brown, J. R.; Laerdahl, J. K.; Stoll, H. *J. Chem. Phys.* **2000**, *113*, 7110. Stoll, H. *Chem. Phys. Lett.* **2006**, *429*, 289.
(34) Grimme, S.; Antony, J.; Ehrlich, S.; Krieg, H. *J. Chem. Phys.* **2010**, *132*, 154104.
(35) Boys, S. F.; Bernardi, F. *Mol. Phys.* **1970**, *19*, 553. Simon, S.; Duran, M.; Dannenberg, J. J. *J. Chem. Phys.* **1996**, *105*, 11024.
(36) Nicu, V. P.; Nuegebauer, J.; Baerends, E. J. *J. Phys. Chem. A* **2008**, *112*, 6978.
(37) Sadlej, J.; Dobrowolski, J. Cz.; Rode, J. E. *Chem. Soc. Rev.* **2010**, *39*, 1478.
(38) Kondo, Y.; Takayanagi, K. *Science* **2000**, *289*, 606.
(39) Merten, C.; Xu, Y. J. *Agnew. Chem., Int. Ed.* **2014**, *52*, 2073.